Localized anharmonic rattling of Al atoms in $VAl_{10.1}$

D. J. Safarik,[1] T. Klimczuk,[1,2] A. Llobet,[1] D. D. Byler,[1] J. C. Lashley,[1] J. R. O'Brien,[3] and N. R. Dilley[3]

[1]*Los Alamos National Laboratory, Los Alamos, New Mexico 87545, USA*

[2]*European Commission, JRC, Institute for Transuranium Elements, Postfach 2340, DE-76125 Karlsruhe, Germany*

[3]*Quantum Design, 6325 Lusk Blvd., San Diego, California 92121, USA*

(Received 7 October 2011; revised manuscript received 28 November 2011; published 5 January 2012)

We have used a suite of diffraction, thermodynamic, and transport measurements to study the localized rattling of Al guest atoms in $VAl_{10.1}$. The mean-square displacement of the rattling atom shows a concave-down temperature dependence. This is characteristic of an anharmonic vibration, the frequency of which increases with amplitude, akin to a particle in a box. We find that the rattling is best described in terms of a sixth-order interatomic potential, with negligible contributions from harmonic and quartic terms. The rattler has a characteristic temperature of $\theta_{RM} = 21$ K and couples strongly to both the acoustic phonons and conduction electrons. The coupling to the phonons is evident from the large value of the Grüneisen parameter, which increases with decreasing temperature to $\Gamma \approx 43$ at 5 K. Below 6 K, the electrical resistivity varies as T^3, which can be explained in terms of electron scattering from damped sixth-order vibrations. $VAl_{10.1}$ is a superconductor below $T_c = 1.53$ K, with an upper critical field of $\sim$1 kG.

DOI: 10.1103/PhysRevB.85.014103 PACS number(s): 61.05.F−, 63.20.Pw, 63.20.Ry, 63.20.kg

I. INTRODUCTION

Localized vibrational states in crystals are usually thought of in relation to extrinsic disorder that breaks the translational invariance of the lattice.[1] Familiar examples include point defects such as substitutional impurities, vacancies, and interstitials.[2,3] In the late 1980s, it was suggested that spatially localized vibrational states could exist even in the absence of such extrinsic disorder.[4–7] These intrinsically localized modes (ILMs), it was proposed, could occur at any lattice site, arising due to the anharmonicity of the effective interatomic potential together with the discreteness of the lattice.[1,4,5] Experimental observations of ILMs have now been reported for several different physical systems of nonlinear coupled oscillators, including arrays of Josephson junctions,[8,9] optical waveguides,[10] and micromechanical resonators.[11] The observation of atomic-scale ILMs in crystals, however, remains more elusive.[12]

Another type of localized mode, characterized by low-frequency vibrations at *specific* crystallographic sites, is now known to exist in several different crystal structures, including the filled skutterudites RM_4Sb_{12} (R = La, Ce, Th, Pr, Tl; M = Fe, Co, Os),[13–16] clathrates such as $X_8Ga_{16}Ge_{30}$ (X = Eu, Sr, Ba),[17,18] $R_3Pd_{20}M_3$ (R = La, Ce, Pr, Nd; M = Si, Ge),[15,19,20] Ba_6Ge_{25},[21,22] and $Na_{24}Si_{136}$,[23] and the β-pyrochlore oxides AOs_2O_6 (A = K, Rb, Cs).[24–26] A common characteristic among these structures is the presence of a three-dimensional network of polyhedral cages, each of which can accommodate one guest atom. When the cage is oversized compared to the guest atom, the guest vibrates anharmonically with low frequency and large amplitude. The vibration can be on center (single-well potential)[17] or off center (multiple-well potential)[15,17–19,21,22,27] relative to the lattice site at the cage center. In the latter case, atomic tunneling or thermally activated relaxation between the multiple wells may play an important role in the mode dynamics.

Most if not all crystals containing these "rattling modes" also show other interesting physics, most notably strong scattering of long-wavelength acoustic phonons,[13,14,17,21] superconductivity,[26,28–31] and sizable electron mass enhancements.[26,29–32] The first phenomenon has in recent years been exploited to develop new skutterudite- and clathrate-based semiconducting thermoelectrics with an enhanced figure of merit owing to the strong suppression of the lattice thermal conductivity.[13,14,17] These materials are often called "electron crystal-phonon glasses." Studies have suggested that the coupling to the acoustic phonons arises from avoided crossings of the guest-atom rattling mode branches with host-lattice acoustic-phonon branches having the same symmetry.[33–36] For the second and third phenomena, superconductivity and electron mass enhancement, the role of the rattling is less clear. It has been suggested that both are mediated by the large excursions of guest atoms from the cage centers that can occur for anharmonic potentials, particularly those with broad, flat bottoms.[26,37,38]

The presence of rattling modes in VAl_{10} was first reported in the early 1970s. Large anomalies in the low-temperature heat capacity, thermal expansion, and electrical resistivity were explained by assuming that VAl_{10} contains a large density of low-energy phonon modes, all with the same Einstein temperature $\theta_E \approx 22$ K.[39–42] The dominance of these low-energy modes was considered so unusual that VAl_{10} was dubbed an "Einstein solid."[39] VAl_{10} was later reported to superconduct below 1.6 K, but the role of Al impurities in the superconductivity was unclear.[43] Although VAl_{10} has been largely forgotten since the late 1970s, the recent discoveries in the clathrate, skutterudite, and β-pyrochlore oxide systems motivate us to reinvestigate this Einstein solid.

$VAl_{10+\delta}$ ($\delta = 0$–0.5) crystallizes in the cubic $Mg_3Cr_2Al_{18}$ structure (Pearson symbol $cF176$, space group $Fd\bar{3}m$).[44,45] As shown in Fig. 1, the structure can be described as a diamond-cubic array of CN16 Frank-Kaspar polyhedra, each of which is vertex connected to four neighboring CN16 polyhedra. There are eight polyhedra per unit cell and two per primitive cell. The array of polyhedra is reinforced by a tetrahedral network of covalently bonded Al-V-Al-V chains that extend over the entire crystal. At each polyhedron center is the 8*a* site, which

can either be empty or be occupied by one Al atom. If none of the 8*a* sites are occupied, the composition is VAl_{10} and the crystal contains 129 optical phonon branches in addition to the three acoustic branches. If all of the 8*a* sites are occupied by Al atoms, the composition is V_2Al_{21} and there six additional optical branches. Ostensibly, these additional branches are the rattling modes. The nearest-neighbor distances from the 8*a* rattling atom site to the polyhedron framework sites are large: 3.16 Å for 8*a*–96*g* and 3.14 Å for 8*a*–16*c*. Thus, the free diameter of the cage, ≈3.5 Å, is appreciably larger than that of even a neutral Al atom, 2.85 Å. This mismatch is evidently the main reason for the rattling. If larger guest atoms occupy the 8*a* site, such as Eu in EuV_2Al_{20} or Gd in GdV_2Al_{20}, the rattling disappears.[46,47]

Another site in the structure, the 16*c* Al site, also has unusually long nearest-neighbor distances. The 16*c* atom is surrounded by a CN14 polyhedron that can be described as a double six-ring polyhedron that is capped in the axial direction. Figure 1 illustrates the CN14 polyhedra and their packing within the unit cell. The distances from the 16*c* site to the polyhedron framework sites, 3.08 Å for 16*c*–96*g* and 3.14 Å for 16*c*–8*a*, are nearly as large as for the CN16 polyhedron. We might therefore expect the 16*c* atoms to also have unusual vibrational characteristics that contribute to the "Einstein solid" behavior.

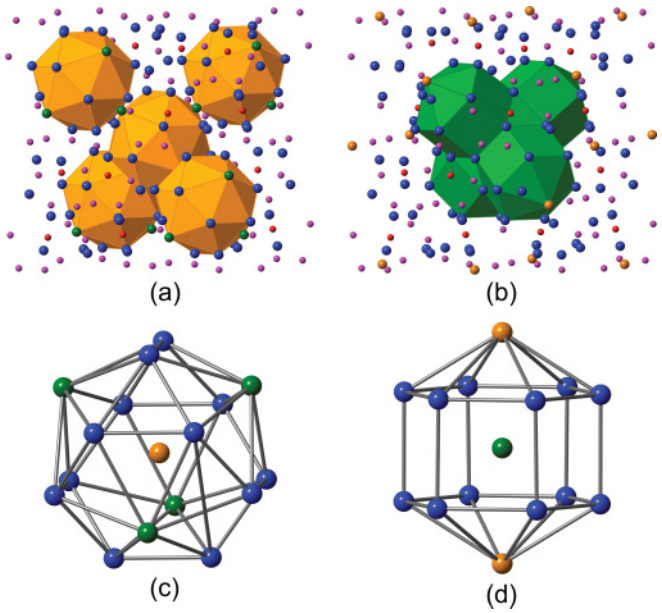

FIG. 1. (Color online) (a), (b) Crystal structure of VAl_{10}, emphasizing (a) the diamondlike array of CN16 Frank-Kaspar polyhedra and (b) the array of CN14 polyhedra. (c), (d) Detailed views of (c) the CN16 coordination polyhedron surrounding the 8*a* Al atom ($\bar{4}3m$ site symmetry), and (d) the CN14 polyhedron surrounding the 16*c* Al atom ($\bar{3}m$ site symmetry). The structure contains four types of Al sites (96*g*, 48*f*, 16*c*, and 8*a*) and one V site (16*d*). The vertices of each CN16 polyhedron are composed of 12 96*g* Al sites (blue spheres online) and 4 16*c* Al sites (green spheres online). Neighboring polyhedra share one 16*c* site. One 8*a* Al site (orange spheres online) occupies the center of each CN16 polyhedron. The vertices of each CN14 polyhedron are composed of 12 96*g* Al sites and 2 8*a* Al sites. One 16*c* Al site occupies the center of each CN14 polyhedron. The 48*f* Al atoms (magenta spheres online) and the 16*d* V atoms (red spheres online) form the reinforcing Al-V-Al-V network. Parts (a) and (b) show one unit cell and are centered on an 8*a* site.

In this paper, we report neutron and x-ray diffraction, heat capacity, thermal expansion, elastic constant, electrical resistivity, and thermal conductivity measurements on polycrystalline $VAl_{10.1}$. We find that the rattling mode is highly anharmonic, with a dominant sixth-order term in the effective interatomic potential. This anharmonicity is associated with strong coupling to the long-wavelength acoustic phonons, as evidenced by large anomalies in the thermodynamic properties. The rattling mode also couples strongly to the conduction electrons, dominating the electron scattering at low temperatures and resulting in an unusual temperature dependence of the resistivity. We have also confirmed the existence of bulk superconductivity in $VAl_{10.1}$ at $T_c = 1.53$ K.

II. EXPERIMENT

Polycrystalline ingots with nominal composition $VAl_{10+\delta}$ ($\delta = 0, 0.10, 0.25, 0.50$, and 0.75) were prepared by arc melting Al pieces (99.999%) and V flakes (99.9%) in a high-purity Ar atmosphere. To ensure homogeneity, we used a multistep melting procedure, first preparing the V-rich intermetallic V_8Al_5 and then adding Al in successive arc-melting steps to form the intermetallic VAl_3 and finally $VAl_{10+\delta}$. The as-cast ingots were wrapped in Ta foil, vacuum sealed in silica tubes ($<10^{-3}$ Torr), and annealed for five days at 650 °C. At the end of the anneal, each sample tube was quenched in −13 °C brine. The ingots were electrodischarge machined into parallelepiped-shaped specimens for thermodynamic and transport property measurements, or ground into powder for x–ray and neutron diffraction measurements.

We characterized the crystal structure of the $VAl_{10+\delta}$ alloys using x-ray and neutron powder diffraction. The x-ray measurements were done at room temperature on a Scintag XDS 2000 diffractometer (Bragg-Brentano θ-θ type), using Cu Kα radiation ($\lambda \approx 0.154\,06$ nm). During each scan, the sample was rotated continuously in the $2\theta = 0°$ plane. The neutron measurements were done on the high-intensity powder diffractometer at the Lujan Neutron Scattering Center at the Los Alamos Neutron Science Center. For these experiments, we used a vanadium sample can to contain approximately 300 mg of $VAl_{10.1}$ powder. Diffraction patterns were measured at seven temperatures between 4 and 300 K. The neutrons were collected in time-of-flight mode using detector banks located at four different angular ranges covering a *d*-spacing range of 0.4–40 Å. All structural refinements were performed using GSAS with the EXPGUI user interface.[48,49] We were particularly interested in deducing from the refinements the temperature dependence of the isotropic mean-squared atomic displacement $\langle u^2 \rangle_{iso}$. Therefore, we were careful to refine the data in as consistent a manner as possible across the $4 \leqslant T \leqslant 300$ K range of our measurements. Specifically, we jointly refined six room-temperature neutron patterns (using banks located at $2\theta = \pm 158°, \pm 90°, \pm 40°$, each covering $\pm 5°$) and one room-temperature x-ray pattern (covering $2\theta = 5°$–$90°$) to determine the values of the Al 8*a* site occupancy, the phase fractions, and nonstructural parameters including the diffractometer constants, the absorption and transmission

corrections, and selected peak-profile parameters. The values deduced from this room-temperature co-refinement were then fixed, and only the lattice parameters, atomic positions, and $\langle u^2\rangle_{\rm iso}$ thermal parameters were refined for all the remaining temperatures.

We measured the heat capacity, thermal expansion, elastic constants, electrical resistivity, and thermal conductivity using a Quantum Design Physical Properties Measurement System. All measurements were done in the range $2 \leqslant T \leqslant 300$ K, except for the heat capacity, where lower temperatures were achieved using dilution and ^{3}He refrigerators. The heat capacity, electrical resistivity, and thermal conductivity measurements were done using standard option packages available from Quantum Design. Resistivity and thermal conductivity measurements were both performed using four-probe techniques, with the lead wires spot welded to the surface of the sample in the case of resistivity and wrapped around and then silver epoxied to the specimen in the case of thermal conductivity.

Thermal expansion was measured using a three-terminal capacitance technique, the details of which are described elsewhere.[50] Data were collected on an Andeen-Hagerling 2700A capacitance bridge. Elastic constants were measured using resonant ultrasound spectroscopy (RUS). In our RUS apparatus, the sample was excited using a Stanford Research Systems (SRS) DS345 function generator driving a lead zirconate titanate (PZT) transducer, and the sample response was detected using a PZT transducer and a SRS SR844 lock-in amplifier. Details of the RUS technique have been discussed in several comprehensive reviews.[51,52]

III. RESULTS

A. Neutron diffraction and the mean-square atomic displacement

Rietveld co-refinements of the x-ray and neutron powder diffraction data confirmed that our $VAl_{10+\delta}$ crystals consisted mainly of the $VAl_{10+\delta}$ phase ($\delta = 0$–0.5) having the cubic $Mg_3Cr_2Al_{18}$-type structure. The crystals also contained a minority phase of pure Al with concentration <5 wt.% for $\delta = 0.1$. With increasing δ, the extra Al formed more impurity phase rather than filling the 8a sites. For this reason, we focus on the $VAl_{10.1}$ alloy for the remainder of the paper. It is difficult to determine the exact composition of the $VAl_{10+\delta}$ phase. However, based on the nominal sample composition of $VAl_{10.1}$ and our heat capacity data (discussed below), we estimate $\delta = 0.05$–0.1.

From the co-refinements of the room-temperature neutron and x-ray data, we concluded that the 8a sites are occupied exclusively, or nearly so, by Al atoms. From these co-refinements, we deduced an 8a occupancy of 0.90. This value was fixed in all subsequent refinements at other temperatures. (The occupancies of the other Al sites and the V site were always fixed at 1.) We should note that this 8a occupancy is larger than the ∼0.20 occupancy that we expected based on the nominal stoichiometry of the alloy. This discrepancy is caused by preferential orientation of the crystallites, which we observed in the neutron image plate measurements.

Here, we are particularly interested in the temperature dependence of the isotropic mean-square atomic displacement $\langle u^2\rangle_{\rm iso}$ for the Al sites. Because in any Rietveld refinement the values of $\langle u^2\rangle_{\rm iso}$ and the site occupancies are correlated, a systematic error in the occupancy will cause a systematic error in the values of $\langle u^2\rangle_{\rm iso}$. However, the *temperature dependence* of $\langle u^2\rangle_{\rm iso}$ will be correct provided that the error in occupancy is unchanged with temperature. This seems to be the case here; by allowing the 8a occupancy to float during all refinements in the range $4 \leqslant T \leqslant 300$ K, we find that its value is constant at 0.90.

To determine $\langle u^2\rangle_{\rm iso}$, each Al site was refined assuming a single-site model using the standard expression for the isotropic Debye-Waller factor $f_{\rm DW} = \exp(-16\pi^2\langle u^2\rangle_{\rm iso}\sin^2\theta/\lambda^2)$, where θ is the diffraction angle and λ the neutron wavelength. Although this expression is rigorously valid only for harmonic vibrations, we have recently shown[53] that even for strongly anharmonic vibrations, the absolute value of $\langle u^2\rangle_{\rm iso}$ deduced using $f_{\rm DW}$ is in error by less than ∼20%. Moreover, the temperature dependence of $\langle u^2\rangle_{\rm iso}$ is nearly correct. This latter point is particularly relevant for the analysis of the 8a site data, as seen below.

Figure 2 shows the temperature dependence of $\langle u^2\rangle_{\rm iso}$ for the four Al atoms in the structure: 96g, 48f, 16c, and 8a (see Fig. 1). The curves through the 96g and 48f data are fits of the Debye-Waller model[54]

$$\langle u^2\rangle_{\rm iso} = \langle u^2\rangle_0 + \frac{3\hbar^2}{mk_B}\left(\frac{1}{4\theta_{\rm DW}} + \frac{T^2}{\theta_{\rm DW}^3}\int_0^{\frac{\theta_{\rm DW}}{T}}\frac{x\,dx}{e^x-1}\right). \quad (1)$$

Here, $\theta_{\rm DW}$ is the Debye-Waller temperature, m is the atomic mass, $\hbar$ and k_B are the Planck and Boltzmann constants, and $\langle u^2\rangle_0$ is a temperature-independent term that accounts for static displacements of the atoms and for systematic errors. Assuming that $m = m_{\rm Al}$, from the fits we deduced $\theta_{\rm DW} = 425$ K and $\langle u^2\rangle_0 \approx 0$ for the 96g atom, and $\theta_{\rm DW} = 725$ K and $\langle u^2\rangle_0 \approx 0$ for the 48f atom.

Here, we should note that the Debye-Waller model assumes a cubic-symmetry lattice site and therefore isotropic atomic displacements. In contrast, the 96g, 48f, and 16c sites have monoclinic, orthorhombic, and trigonal symmetries, respectively, and thus the displacements are anisotropic. (The 8a site has cubic symmetry.) As pointed out by Willis and Pryor,[55] our present use of Eq. (1) is justified because in our Rietveld refinement, we interpreted the thermal factors in terms of the isotropic model, thereby deducing "equivalent" or "quasicubic" values of $\langle u^2\rangle_{\rm iso}$. Similar comments apply to our use of the Einstein model, discussed below.

The Debye-Waller model also assumes that all phonon modes contributing to $\langle u^2\rangle_{\rm iso}$ are harmonic and acoustic, with a partial phonon density of states (DOS) given by the Debye approximation $D(\omega) \propto \omega^2$. For $VAl_{10+\delta}$, which has only 3 acoustic branches but 129–135 optical phonon branches (depending on the value of δ), the assumption of a Debye DOS is probably unrealistic. For this reason, we also fitted our data using an Einstein model $\langle u^2\rangle_{\rm iso} = \langle u^2\rangle_0 + (\hbar^2/mk_B\theta_E)\coth(\theta_E/2T)$, where θ_E is the Einstein temperature. We found that the data are described equally well by the Debye-Waller and Einstein models, but the characteristic temperatures are different: using the Einstein

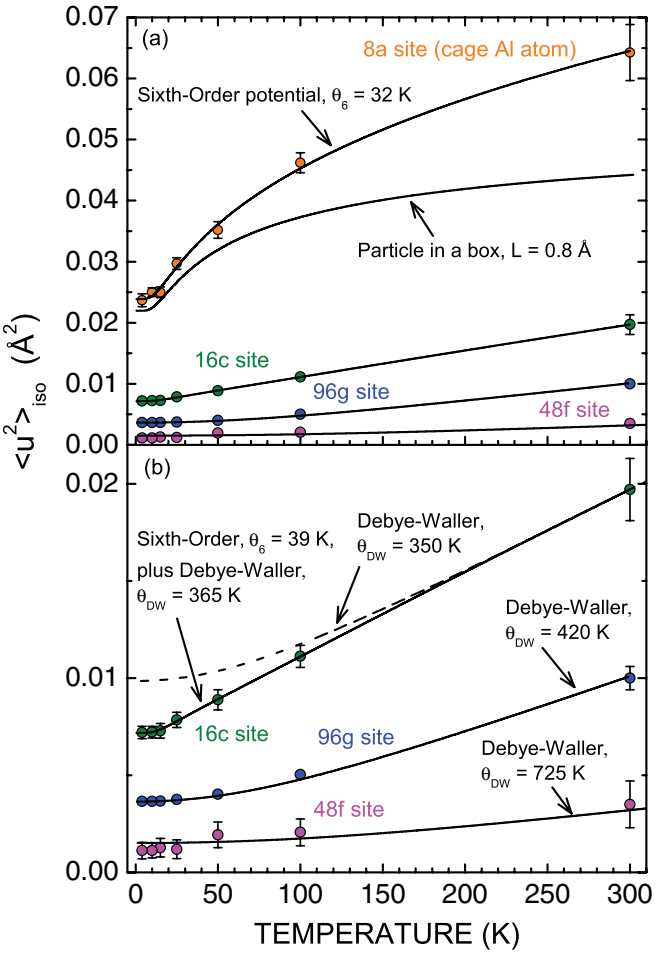

FIG. 2. (Color online) (a), (b) Temperature dependence of the isotropic mean-square atomic displacement $\langle u^2\rangle_{\rm iso}$ for the different Al atoms, as determined from Rietveld refinement of neutron diffraction data. Error bars are shown only when larger than the size of the points. The curves through the 96*g* and 48*f* data are fits of the Debye-Waller model [Eq. (1)] for harmonic acoustic phonons. The curve through the 8*a* data is the fit for a sixth-order optical phonon. The solid curve through the 16*c* data is the fit for a sixth-order anharmonic phonon plus the Debye-Waller model [Eq. (2)].

model, $\theta_E = 240$ K for the 96*g* atom and $\theta_E = 420$ K for 48*f*. These values are smaller than the Debye-Waller temperatures by a factor of $\sqrt{3}$. This is due to the different vibrational spectra assumed for the two models. Aside from this difference, the details of the phonon DOS evidently have little effect on the temperature dependence of $\langle u^2\rangle_{\rm iso}$. Most likely, the reason is that the zero-point mean-square displacement is proportional to the first moment of the phonon DOS, and hence is fixed mainly by the highest-frequency modes in the spectrum.[56]

Compared to the 96*g* and 48*f* atoms, for the 8*a* atom the magnitude of $\langle u^2\rangle_{\rm iso}$ is much larger. Clearly, the 8*a* Al atom is the "rattling atom" in $VAl_{10+\delta}$. As seen in Fig. 2, the most interesting feature of the 8*a* data is its concave-down temperature dependence, which is completely different than that of a harmonic vibration. We will now show that this concavity is the signature of an anharmonic phonon, the frequency of which increases with vibrational amplitude.

Based on the structure of $VAl_{10.1}$, namely, the presence of a "rattling" atom in an oversized cage, we can as a first approximation model the 8*a* atom as a particle in a box. This is a limiting case for an anharmonic single-well potential. Using the interatomic distances deduced from our diffraction data, we estimate that for neutral and hard-sphere Al atoms, the box dimension is $L \approx 0.7$–0.8 Å. From the well-known wave functions Ψ_n and eigenenergies E_n for the eigenstates n, we compute $\langle u^2\rangle_{\rm iso}$ numerically from $\langle u^2\rangle_{\rm iso} = \sum_n p_n \langle\Psi_n|u^2|\Psi_n\rangle$, where $p_n = e^{-\beta E_n}/Z$ is the Boltzmann weight, $Z = \sum_n e^{-\beta E_n}$ is the partition function, $\beta = 1/k_B T$, and u is the displacement from the center of the well. For $L = 0.8$ Å and a particle of mass $m_{\rm Al}$, we calculate the curve shown in Fig. 2. Clearly, the particle-in-a-box model reproduces qualitatively the concave-down temperature dependence of our $\langle u^2\rangle_{\rm iso}$ data. The physical interpretation of the concavity, then, is that the displacement of the 8*a* atoms is restricted by the cage walls.

For increasing temperature, the particle-in-a-box model predicts that $\langle u^2\rangle_{\rm iso}$ approaches a saturation value. Our data, however, show a $T^{1/3}$ dependence from 25 K up to 300 K, with no sign of saturation. This T dependence is characteristic of sixth-order (sextic) potential, rather than a square well.[57] We obtain favorable agreement with our data over the entire range $4 < T < 300$ K by modeling the rattling modes as sextic vibrations, with interatomic potential $V(u) = \frac{1}{6}(m^3\omega_{RM,6}^4/\hbar^2)u^6$ and characteristic frequency $\omega_{RM,6}$. This is shown in Fig. 2, where the curve through the 8*a* data is the fit of $\langle u^2\rangle_{\rm iso} = \langle u^2\rangle_0 + \sum_n p_n\langle\Psi_n|u^2|\Psi_n\rangle$ for the sextic oscillator. The wave functions Ψ_n and eigenenergies E_n used in the fit were obtained by numerically solving the Schrödinger equation. From the fit, we determined $\theta_{RM,6} = \hbar\omega_{RM,6}/k_B = 32$ K, $m = 1.07 m_{\rm Al}$, and $\langle u^2\rangle_0 = 0.0033$ Å^2. For the purely sixth-order oscillator, this value of $\theta_{RM,6}$ equates to characteristic temperatures of 40, 59, and 73 K for the level transitions $0 \to 1$, $1 \to 2$, and $2 \to 3$, respectively. Based on the value of $\langle u^2\rangle_0$ found here, we can not rule out the possibility of static disordering of the 8*a* atoms. However, if the 8*a* atoms vibrate in single-well potentials and the lattice has little or no distortion, as are suggested by our diffraction and heat capacity data, then the static contribution to $\langle u^2\rangle_{\rm iso}$ should be small compared to the dynamic one.

Finally, we consider the data for the 16*c* atom. As shown in Fig. 2(b), $\langle u^2\rangle_{\rm iso}$ decreases linearly with temperature down to 15 K, and then remains virtually unchanged on further cooling to 4 K. The linearity of high-temperature data implies that the vibrations are harmonic. However, we were unable to fit the data using only the harmonic Debye-Waller or harmonic Einstein model. The problem is that the value of θ required to explain the slope of the high-temperature data can not also explain why the zero-point saturation of $\langle u^2\rangle_{\rm iso}$ occurs at such a low temperature, $T \approx 15$ K. This is demonstrated in Fig. 2(b), where the dashed curve is the Debye-Waller model for $\theta_{\rm DW} = 350$ K, which is the value deduced from the high-temperature slope. The 15 K saturation temperature suggests the presence of additional excitations with lower characteristic energy.

The data could be fitted by assuming two contributions to the 16*c* partial density of states: one from harmonic acoustic (Debye) modes, and one from *anharmonic* low-frequency optical modes. The data can not be fitted by assuming that the

optical modes are harmonic. We modeled the optical modes as sextic vibrations, just as for the neighboring 8*a* rattling site. In this case,

$$\langle u^2\rangle_{\rm iso} = \langle u^2\rangle_0 + f\sum_n p_n\langle\Psi_n|u^2|\Psi_n\rangle + (1-f)\frac{3\hbar^2}{mk_B}\left(\frac{1}{4\theta_{\rm DW}} + \frac{T^2}{\theta_{\rm DW}^3}\int_0^{\frac{\theta_{\rm DW}}{T}}\frac{x\,dx}{e^x-1}\right), \quad (2)$$

where f is the fraction of the 16*c* modes that are strongly anharmonic. The fit of Eq. (2) to the 16*c* data is shown in Fig. 2. From the fit, we determined $\theta_{RM,6} = 39$ K, $\theta_{\rm DW} = 365$ K, $f = 0.148$, and $\langle u^2\rangle_0 = 0.0013$ Å^2. This value of $\theta_{RM,6}$ is close to that deduced for the neighboring 8*a* rattling atom, i.e., $\theta_{RM,6} = 32$ K. Furthermore, the value of f seems to be physically meaningful when interpreted in terms of the crystal structure. Recall that the primitive cell of $VAl_{10+\delta}$ contains 44–46 atoms, 4 of which are 16*c* Al atoms, and 0–2 of which are 8*a* Al atoms depending of the value of δ. We estimate that $\delta = 0.05$–0.1 for the $VAl_{10+\delta}$ phase of our crystal, meaning that each primitive cell contains on average 0.2–0.4 Al atoms in the 8*a* site. Of the four 16*c* atoms per primitive cell, on average, 0.6–1.2 of them are nearest neighbors of *occupied* 8*a* sites. This fraction, $0.6/4 = 0.15$ to $1.2/4 = 0.30$, is comparable to $f = 0.148$ that we found by fitting Eq. (2) to the data. Thus, one interpretation of the data is that 16*c* atoms neighboring *occupied* 8*a* sites vibrate anharmonically, presumably due to coupling to adjacent 8*a* rattling atoms, whereas 16*c* atoms neighboring *unoccupied* 8*a* sites vibrate harmonically.

B. Thermodynamic properties

1. Heat capacity

Figure 3 shows the temperature dependence of the (a) heat capacity (plotted as C_p/T), (b) coefficient of linear thermal expansion, (c) elastic constants, and (d) Grüneisen parameter. All thermodynamic properties show large anomalies that extend from 2 K upward to 50 and even ~100 K in the case of the elastic constants. From the heat capacity data, one can immediately infer a large density of states of excitations with characteristic temperature less than 50 K. From the thermal expansion, elastic constants, and Grüneisen data, we can further infer that the rattling modes couple strongly to the acoustic phonons, which is consistent with the anharmonicity evident in the $\langle u^2\rangle_{\rm iso}$ data.

To analyze the low-temperature heat capacity data, we must assume that aside from the usual contributions from the electrons and acoustic (Debye) phonons, there is an additional contribution from non-Debye vibrations. We model these vibrations as sextic, just as for our analysis of the $\langle u^2\rangle_{\rm iso}$ data. In this case, the heat capacity is

$$C_p = \gamma T + \frac{12\pi^4}{5\theta_D^3}(N - N_{RM})k_B T^3 + 3N_{RM}C_{v,RM}, \quad (3)$$

where γ is the Sommerfeld coefficient, θ_D is the Debye temperature, N is the number of atoms is the solid, N_{RM} is the number of rattling atoms, and $C_{v,RM}$ is the heat capacity of one sextic vibration with characteristic temperature $\theta_{RM,6}$. The curve through the data in Fig. 3(a) shows the fit of Eq. (3) in the range $0.01 < T < 25$ K. We should note that comparable fits are found using harmonic and quartic oscillators since the computed $C_p(T)$ is somewhat insensitive to the anharmonicity. The fact that Eq. (3) can be fitted over a large temperature range, up to $T/\theta_D \approx 1/14$, reflects the dominant contribution of the rattling modes to the low-energy phonon DOS. This is also evident from the dashed curves in Fig. 3(a), which show the contributions from only the electrons plus the Debye phonons. From the fit of Eq. (3), we deduced $\gamma = 1.56$ mJ mol atoms^{-1} K^{-2}, $\theta_D = 341$ K, $\theta_{RM,6} = 21$ K, and $N_{RM}/N = 0.014$. This value of N_{RM}/N is larger than 0.01, which is the fraction of atoms occupying the 8*a* site in $VAl_{10.1}$. This might reflect the participation of additional atoms aside from the 8*a*, for example, the 16*c* atoms, as suggested by the $\langle u^2\rangle_{\rm iso}$ data in Fig. 2. The characteristic temperature of 21 K is close to 32 K, which is the value of $\theta_{RM,6}$ determined from our analysis of the $\langle u\rangle_{\rm iso}$ data. It also agrees well with the value of 22 K deduced by Caplin and co-workers,[39,41] who used a harmonic (Einstein) model to interpret their heat capacity data. We should note that the frequency of the rattling in $VAl_{10.1}$ is among the lowest among all known rattling-mode materials. This is interesting considering the small mass of the Al guest. To our knowledge, only the 150% more massive Ga guest in Ga-doped VAl_{10} has a lower frequency, with $\theta \approx 8$ K.[41,42] The 50% more massive K guest in KOs_2O_6, with $\theta \approx 22$ K,[31] has a comparable frequency to the Al guest in $VAl_{10.1}$.

As pointed out by Caplin and Nicholson,[41] in Ga-doped VAl_{10}, the characteristic temperature for the Ga rattler is about 0.4 that of the Al rattler, whereas the mass ratio of Al to Ga is 0.38. They noted that disregarding any change in the interatomic potential, this mass scaling would be expected for a rotator or a square-well potential (m^{-1}), but not for a harmonic oscillator ($m^{-\frac{1}{2}}$). This is consistent with the present picture of a sextic (square-well-like) potential for the Al rattler in $VAl_{10.1}$

We have also measured the heat capacity down to 100 mK, using ^{3}He and dilution refrigerators. These data are shown in Fig. 4. The main panel shows C_p/T versus $\log T$, measured at both zero applied field and at 1 kG. The shoulder near 10 K is due to excitation of the rattling modes. At lower temperatures, near 1.53 K, $VAl_{10.1}$ undergoes a superconducting transition. The magnitude of the heat capacity jump suggests that the superconductivity has bulk character and is not associated with the Al impurity. We have not studied the field dependence of T_c in detail, but the transition is suppressed to $T_c < 100$ mK by applying a field between 0.8 and 1 kG. For 1 kG, the C_p/T versus T data is flat and featureless below ~2 K, as expected when normal-state electrons dominate the heat capacity.

The inset of Fig. 4 shows the temperature dependence of the electronic heat capacity, plotted as C_e/T, near the superconducting transition. Here, the phonon component was estimated by fitting Eq. (3) to the normal-state data, as done previously, only now we used two sextic oscillators to obtain a better estimate of the phonon contribution. The superconducting transition temperature, as determined from an entropy-conserving construction, is $T_c = 1.53$ K. This falls within the range of T_c's determined previously for VAl_{10} via inductance measurements.[43] The sharpness of the transition $\Delta T_c \approx 0.2$ K suggests that our $VAl_{10.1}$ polycrystals

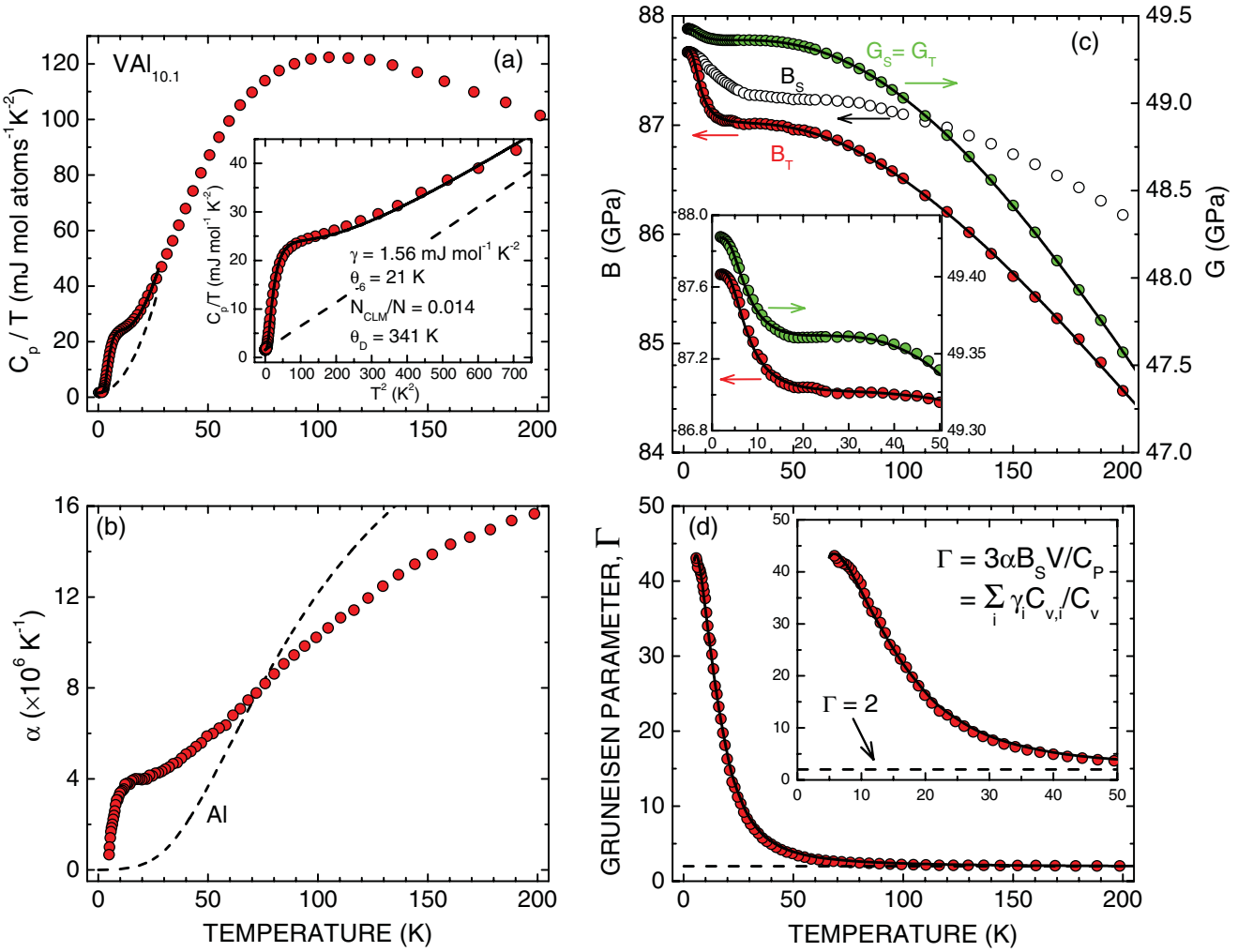

FIG. 3. (Color online) Temperature dependence of the thermodynamic properties of $VAl_{10.1}$: (a) heat capacity, plotted as C_p/T, (b) coefficient of linear thermal expansion, (c) adiabatic bulk (B_S), isothermal bulk (B_T), and adiabatic and isothermal shear ($G_S = G_T$) moduli, and (d) thermodynamic Grüneisen parameter, all measured at zero applied magnetic field. The curves through the C_p/T, G_T, B_T, and Γ data are fits of Eqs. (3), (4), (5), and (6), respectively.

are homogeneous and of good quality. Based on the equal-entropy analysis, we determined a heat capacity jump of $\Delta C_e/\gamma T_c = 1.42$. This is close to 1.43, which is the value predicted by BCS theory for weak coupling.[58]

2. *Thermal expansion*

As shown in Fig. 3(b), the thermal expansion coefficient rises steeply above 5 K, has a shoulder in the range $15 < T < 25$ K, and then continues to increase at a slower rate above 25 K. The temperature of the shoulder is approximately equal to the $\theta_{RM,6} = 21$ K characteristic temperature deduced from the heat capacity data. More interestingly, the value at the shoulder, $\alpha \approx 4 \times 10^{-6}$ K^{-1}, is 10 to 40 times larger than that of pure Al (dashed curve) in the same temperature range. These data are qualitatively similar to those measured by Legg and Lanchester.[42] The large value of α, together with the low temperature of the plateau, points to the strong coupling of the anharmonic rattling mode to nondeviatoric (volume-changing but shape-conserving) thermal strains, and hence to the long-wavelength longitudinal and transverse acoustic modes.

3. *Elastic constants*

The temperature dependence of the elastic constants mirrors that of the thermal expansion coefficient. This is shown in Fig. 3(c), where we plot data for the two independent moduli of polycrystalline $VAl_{10.1}$. Here, we choose the shear modulus G and the bulk modulus B as the independent moduli because they characterize the response to purely deviatoric (shape-changing but volume-conserving) and purely nondeviatoric (volume-changing but shape-conserving) deformations, respectively. We include in Fig. 3(c) data for both the adiabatic and isothermal moduli. The adiabatic moduli G_S and B_S were measured directly using resonant ultrasound spectroscopy. For moduli associated with purely deviatoric deformations, the isothermal and adiabatic values are equal, so $G_T = G_S$.[59] For moduli associated with deformations having a nondeviatoric component, they are different. In the case of the bulk modulus, $B_T = B_S/\left(1 + T\beta^2 B_S V/C_p\right)$,[60]

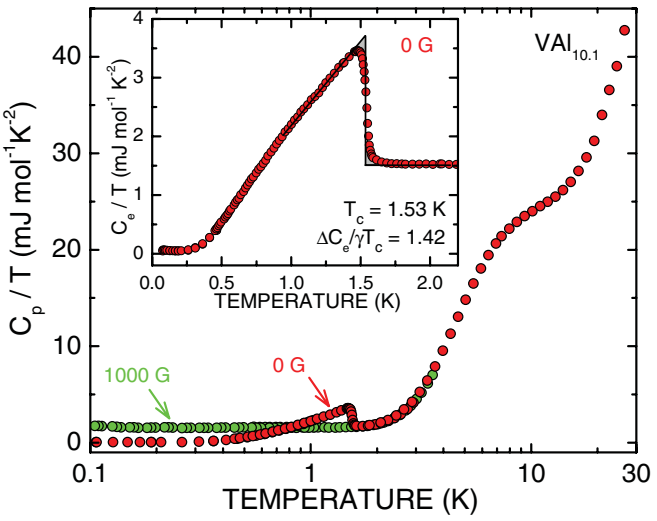

FIG. 4. (Color online) Main panel: Temperature dependence of C_p/T, measured at zero applied field and 1 kG. Inset: Temperature dependence of the electronic heat capacity, plotted as C_e/T, near the superconducting transition. Note the different scales.

where β is the volume thermal expansion coefficient ($\beta = 3\alpha$ for $VAl_{10.1}$). For most materials, the difference between B_T and B_S is negligible. However, because of its huge thermal expansion coefficient at low temperatures, for $VAl_{10.1}$ the difference is large, reaching 2% at 200 K. This results in a substantially different temperature dependence for B_S and B_T, which is particularly important when extracting the coupling coefficients from these data, which we do next.

The T dependence of the moduli suggest that the rattling modes couple strongly to externally applied deformations, and hence to the $k = 0$ longitudinal acoustic (LA) and transverse acoustic (TA) phonons. Here, we use a simple quasiharmonic model to quantify the strength of the coupling. Within the quasiharmonic approximation, the T dependence of the isothermal shear and bulk moduli are[59]

$$G_T(T) = G(0) - A_1T^2 + K_1\frac{\Delta L(T)}{L} + \frac{1}{V}\left(\left\langle\frac{1}{\omega_{Ph}}\frac{\partial^2\omega_{Ph}}{\partial\epsilon_G^2}\right\rangle U_{Ph} - \left\langle\left(\gamma_{Ph}^G\right)^2\right\rangle TC_{v,Ph}\right) + \frac{3N_{RM}}{V}\left(\frac{1}{\omega_{RM,6}}\frac{\partial^2\omega_{RM,6}}{\partial\epsilon_G^2}U_{RM} - \left(\gamma_{RM}^G\right)^2TC_{v,RM}\right) \quad (4)$$

and

$$B_T(T) = B(0) - A_2T^2 + K_2\frac{\Delta L(T)}{L} + \frac{1}{V}\left(\left\langle\frac{1}{\omega_{Ph}}\frac{\partial^2\omega_{Ph}}{\partial\epsilon_V^2}\right\rangle U_{Ph} - \left\langle\left(\gamma_{Ph}^V\right)^2\right\rangle TC_{v,Ph}\right) + \frac{3N_{RM}}{V}\left(\frac{1}{\omega_{RM,6}}\frac{\partial^2\omega_{RM,6}}{\partial\epsilon_V^2}U_{RM} - \left(\gamma_{RM}^V\right)^2TC_{v,RM}\right). \quad (5)$$

In Eqs. (4) and (5), the first term on the right is the value of the modulus at 0 K. The second term is the electronic contribution, where A_1 and A_2 are constants. The third term accounts for the *implicit* dependence of the phonon frequencies and the lattice potential energy on thermal expansion. Here ,K_1 and K_2 are effective moduli that represent the sum of several second- and third-order elastic constants,[61] and $\Delta L(T)/L$ is the relative length change due to thermal expansion. The remaining terms on the right account for the *explicit* dependence of the phonon frequencies on the *externally* applied strain. In these last terms, we have divided the phonons into two groups: rattling modes and background modes. The quantities U_{Ph} and $C_{v,Ph}$ are the internal energy (relative to 0 K) and heat capacity for the phonon background, whereas U_{RM} and $C_{v,RM}$ are the same quantities for one sextic rattling mode. The mode Grüneisen parameters $\gamma_{RM}^{G,V} = -\omega_{RM,6}^{-1}(\partial\omega_{RM,6}/\partial\epsilon_{G,V})$ and the second derivatives $\omega_{RM,6}^{-1}(\partial^2\omega_{RM,6}/\partial\epsilon_{G,V}^2)$ characterize the coupling of the rattling mode to the shear strain ϵ_G and volume strain ϵ_V. Similarly, the mode-averaged Grüneisen parameters $\langle(\gamma_{Ph}^{G,V})^2\rangle = \sum_j(-\omega_j^{-1}\partial\omega_j/\partial\epsilon_{G,V})^2 C_{v,j}/\sum_j C_{v,j}$ and $\langle\omega_{Ph}^{-1}\partial^2\omega_{Ph}/\partial\epsilon_{G,V}^2\rangle = \sum_j(\omega_j^{-1}\partial^2\omega_j/\partial\epsilon_{G,V}^2)C_{v,j}/\sum_j C_{v,j}$ characterize the average coupling of the $3(N - N_{RM})$ background phonon modes.

The curves in Fig. 3(c) show the fits of Eqs. (4) and (5) to the data. For these fits, we used values of $\Delta L(T)/L$ obtained from our thermal expansion data. The heat capacity $C_{v,RM}$ was assumed to be that of a sextic oscillator with $\theta_{RM,6} = 21$ K and number density was $N_{RM}/N = 0.014$, as determined from the heat capacity data. The background phonon heat capacity was computed from $C_{v,Ph} = C_v - \gamma T - 3N_{RM}C_{v,RM}$, where C_v is the measured total heat capacity and $\gamma = 1.56$ J mol^{-1}K^{-2}. Internal energies U_{RM} and U_{Ph} were obtained by integrating the respective heat capacities. Using these thermodynamic data, and further noting that (i) to first order $\langle(\omega_{Ph}^{-1}(\partial^2\omega_{Ph}/\partial\epsilon_{G,V}^2)\rangle = \langle(\gamma_{Ph}^{G,V})^2\rangle$, and (ii) the electronic T^2 terms can be omitted with little error, Eqs. (4) and (5) each have five parameters to be determined by fitting to the data. From the shear modulus data, we found $\langle(\gamma_{Ph}^G)^2\rangle = 0.7$ for the background phonons, and $\gamma_{RM}^G = 24$ and $\omega_{RM,6}^{-1}(\partial^2\omega_{RM,6}/\partial\epsilon_G^2) = 31$ for the rattling modes. From the bulk modulus data, we determined $\langle(\gamma_{Ph}^B)^2\rangle = 2.1$ for the background phonons, and $\gamma_{RM}^V = 73$ and $\omega_{RM,6}^{-1}(\partial^2\omega_{RM,6}/\partial\epsilon_V^2) = 78$ for the rattlers. It is important to note that we determined these values using $N_{RM}/N = 0.014$. This corresponds to a stoichiometry of $VAl_{10.15}$ for the $VAl_{10+\delta}$ phase. If we instead use a stoichiometry of $VAl_{10.1}$, as implied by our sample composition (assuming no Al impurity), we find that the mode Grüneisen parameters are 50% larger than the values stated here.

Interestingly, from our analysis, we find that for $T \gtrsim 100$ K the temperature dependence of B_T and G_T arises mainly from expansion of the lattice, e.g., the $\Delta L(T)/L$ terms in Eqs. (4) and (5). Conversely, for $T \lesssim 100$ K, it is due mainly to the strong coupling of the rattling-mode frequency to the applied strain, and hence to the LA and TA phonons. This coupling is a consequence of the rattling mode's huge anharmonicity.

4. Grüneisen parameter

Figure 3(d) shows the temperature dependence of the thermodynamic Grüneisen parameter $\Gamma = 3\alpha B_S V/C_p$. For temperatures above 200 K, Γ approaches a limiting value of $\sim$2. With decreasing temperature, Γ increases steeply,

reaching a value of ~43 at 5 K, the lowest temperature for which we have thermal expansion data. The Grüneisen Γ is equivalent to the weighted average of the mode Grüneisen parameters[60] $\Gamma = \sum_i \gamma_i C_{v,i} / \sum_i C_{v,i}$, where the sums are over all excitations in the solid. For the present analysis, we classify the excitations into three types: electrons, background phonons, and anharmonic rattling modes. In this case,

$$\Gamma = \frac{\gamma_e^V C_e + \langle \gamma_{Ph}^V \rangle C_{v,Ph} + \gamma_{RM}^V N_{RM} C_{v,RM}}{C_v}, \qquad (6)$$

where $\gamma_e^V = [V/D(\epsilon_F)][\partial D(\epsilon_j)/\partial V]$ is the electronic Grüneisen parameter, $D(\epsilon_F)$ is the density of states at the Fermi level, C_e is the electronic heat capacity, C_v is the total heat capacity, and $\langle \gamma_{Ph}^V \rangle$ is the mode-averaged Grüneisen parameter for the background phonons, the definition of which is analogous to that for $\langle (\gamma_{Ph}^V)^2 \rangle$.

The curve through the data in Fig. 3(d) shows the fit of Eq. (6). In this fit, we used the same data and parameters used for the elastic constant analyses. We also assumed that $\gamma_e^V = 1.8$, the value for pure Al.[60] This left only two parameters to be determined by fitting, for which we deduced $\langle \gamma_{Ph}^V \rangle = 1.5$ and $\gamma_{RM}^V = 54$. Both values are comparable to those determined from the bulk modulus data $\sqrt{\langle (\gamma_{Ph}^V)^2 \rangle} = 1.45$ and $\gamma_{RM}^V = 73$. Recall, however, that these values may be 50% too small because of the uncertainty in the composition of the $VAl_{10+\delta}$ phase.

C. Transport properties

1. *Electrical resisitivity*

Figure 5 shows the temperature dependence of the electrical resistivity. Above ~80 K, the data show a downward concavity suggesting that $\rho(T)$ saturates for $T > 300$ K. Similar concavity has been measured for other metallic rattling-mode materials, for example, the β-pyrochlores AOs_2O_6 (A = K, Cs, Rb) (Ref. 26) and the filled skutterudite $PrOs_4Sb_{12}$.[29] The downward concavity is in qualitative agreement with the models of Mahan and Sofo[57] and Dahm and Ueda,[62] who calculated $\rho(T)$ due to scattering by anharmonic phonons. They found that, for anharmonic potentials $V(u) \propto u^n$, where $n = 4,6,8$, the temperature dependence is $\rho \propto T^{2/n}$ in the high-temperature limit. Our $VAl_{10.1}$ data, however, show no such power-law dependence for $80 < T < 300$ K. This differs from KOs_2O_6, $RbOs_2O_6$, and $CsOs_2O_6$, which all show a $\sqrt{T}$ dependence above 100 K.[26]

The resistivity of poorly conducting metals often shows a concave-down temperature dependence.[63] In that sense, the concavity observed for $VAl_{10.1}$, the β-pyrochlores, and $PrOs_4Sb_{12}$ is not surprising, considering that these alloys all have room-temperature resistivites of ⩾100 μΩ cm. The resistivity of such metals is often well described by the phenomenological "shunt" model $1/\rho(T) = 1/\rho_{\text{ideal}}(T) + 1/\rho_{\max}$.[63] Here, $\rho_{\text{ideal}}(T)$ is the ideal resistivity arising from electron-impurity, electron-electron, electron-phonon, etc., scattering and $\rho_{\max}$ is the maximum limiting resistivity. The curve through the data in Fig. 5(a) shows the fit of the shunt model in the range $90 < T < 300$ K. For this analysis, we assumed that ρ_{ideal} is dominated by electron-harmonic phonon scattering in the high-temperature limit, so that $\rho_{\text{ideal}} = a + bT$ as given by Bloch-Grüneisen theory. From the fit, we determined a saturation resisitivity of $\rho_{\max} = 188$ μΩ cm.

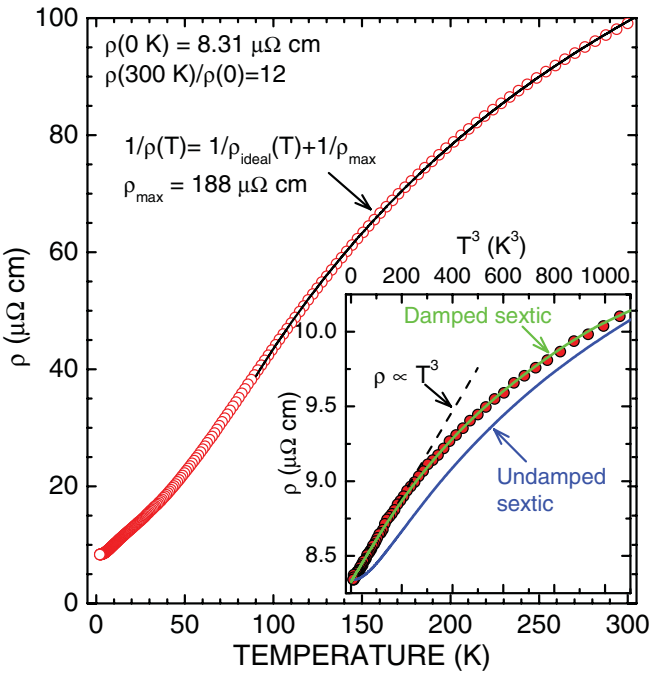

FIG. 5. (Color online) Temperature dependence of the resistivity of $VAl_{10.1}$, plotted as ρ vs T in the main panel and ρ vs T^3 in the inset. Below 40 K, the rattling mode makes the main contribution to the temperature dependence. For $T < 12$ K, the data are well described by a simple model of electron scattering by a damped sextic vibration.

On cooling to 40 K, the slope $d\rho/dT$ abruptly decreases. Most likely, in this temperature range, scattering by the rattling modes becomes increasingly dominant because the density of other phonon states with comparably low energies ($\theta_{RM,6} = 21$ K) is small. In the range $2 < T < 6$ K, the resistivity shows a T^3 dependence. This is seen in the inset, where we plot ρ versus T^3. To our knowledge, a T^3 dependence has not been seen for other rattling-mode materials, although a T^2 dependence at low temperatures has been reported for AOs_2O_6 (A = K, Rb, Cs).[26] In what follows, we show that the low-temperature resistivity data, including the T^3 regime, can be explained in terms of electron scattering by a damped sextic vibration.

To calculate the contribution of the rattling modes to the resistivity, we follow closely the work of Mahan and Sofo,[57] except here we assume that the anharmonic phonon is damped owing to the interaction with conduction electrons.[62] In this case, the phonon spectral function is

$$A(\omega) = \sum_v f_v \frac{1}{\pi} \frac{4\Omega_v \Gamma_0 \omega}{\left(\omega^2 - \Omega_v^2\right)^2 + 4\Gamma_0 \omega^2}, \qquad (7)$$

where ω is the frequency, $\Omega_v = (E_{n+k} - E_k)/\hbar$ is the frequency of the transition v between states with eigenergies E_n and E_{n+k}, and Γ_0 is the temperature-independent phonon damping rate. The strength of a particular transition is

$$f_v = \frac{1}{Z}(e^{-\beta E_n} - e^{-\beta E_{n+k}})\langle n|\xi|n+k\rangle^2, \qquad (8)$$

where Z is the partition function, $\langle n|\xi|n+k\rangle$ is the relevant matrix element for the electron-phonon interaction in the adiabatic approximation, and ξ is the dimensionless displacement as defined previously. Since the matrix elements decrease rapidly with increasing k, it is an accurate approximation to consider only $k = 1$,[57] which we do here. Calculation of the resistivity requires the energy-dependent electron lifetime, which is proportional to the imaginary part of the retarded electronic self-energy[62]

$$\tau^{-1}(\epsilon) \propto \int_0^\infty A(\Omega)[2n_B(\Omega) + f(\Omega+\epsilon) + f(\Omega-\epsilon)]d\Omega, \tag{9}$$

where ϵ is the electron energy and $n_B(\Omega) = (e^{\beta\hbar\Omega} - 1)^{-1}$ and $f(\Omega) = (e^{\beta\hbar\Omega} + 1)^{-1}$ are the Bose and Fermi distributions, respectively. The temperature dependence of the lifetime is then obtained by averaging $\tau(\epsilon)$ over the electron energies $\tau(T) = -\int_{-\infty}^{\infty} \frac{df}{d\epsilon}\tau(\epsilon)d\epsilon$. The resistivity is calculated from $\rho(T) = D\tau^{-1}(T)$, where D is a fitting parameter.

Using the previously determined eigenfunctions Ψ_n and eigenergies E_n for a sextic oscillator with $\theta_{RM,6} = 21$ K, together with the above equations, we have calculated $\rho(T)$ numerically for different values of the damping rate Γ_0. We find that the low-temperature behavior of our $\rho(T)$ data, including the T^3 regime, can be reproduced for $\Gamma_\theta = \hbar\Gamma_0/k_B = 4$ K. This is demonstrated by the curve in the Fig. 5 inset, which fits the data well up to ~12 K. For $T > 12$ K, contributions from other scattering mechanisms evidently become important and the resistivity rises more quickly than predicted by this simple model.

Using an approach similar to the present one, Dahm and Ueda[62] showed that for a damped *quartic* vibration, the resistivity varies as T^2 at low temperatures, in agreement with data for the β-pyrochlore oxides AOs_2O_6, (A = K, Rb, Cs).[26]

2. *Thermal conductivity*

Figure 6 shows temperature dependence of the thermal conductivity κ. For $T < 6$ K, κ increases linearly with temperature, as expected when electrons are the dominant mechanism of heat transport. Using the Wiedemann-Franz law, $\kappa_e = L\rho^{-1}T$, together with our electrical resistivity data and the Lorenz number $L = 2.45 \times 10^{-8}$ W Ω K^{-2}, we calculated the electronic contribution to the conductivity, shown by the curve in Fig. 6. This simple calculation captures the temperature dependence seen in the data, although the computed values of κ are too large. Based on this analysis, it is safe to assume that the lattice contribution to the conductivity is small compared to the electronic one.

IV. DISCUSSION

A. Anharmonicity of the rattling modes and their coupling to the acoustic phonons

The concave-down temperature dependence of $\langle u^2\rangle_{\rm iso}$ observed for the 8*a* rattling atom is a clear signature for strong anharmonicity of at least one of its three optical modes. That the concavity is to the abscissa rather than to the ordinate implies that the frequency increases with amplitude, e.g., the vibration can be described qualitatively as a particle in a box. More quantitatively, we have found that the rattling is best described using a sextic vibration, with negligible contributions from harmonic and quartic terms. The idea that the Al atom rattles anharmonically was first proposed in the 1970s. Based on pseudopotential calculations, Caplin and Nicholson[41] proposed that the 8*a* site was actually fourfold split, with each minimum located about 0.55 Å from the cage center on a spherical surface having slightly greater potential energy. The picture that emerged, then, was one of a quasifree rotator. At the time there was no clear experimental evidence to support Caplin and Nicholson's anharmonic model.

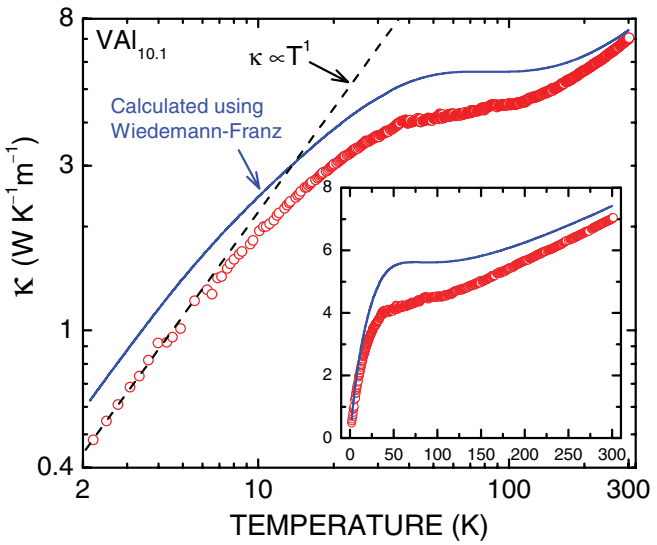

FIG. 6. (Color online) Temperature dependence of the thermal conductivity, plotted in log-log and linear-linear forms. The solid curve shows the conductivity calculated from the resistivity data in Fig. 5, using the Wiedemann-Franz law. The end of the plateau at ~115 K corresponds to the onset of electrical resistivity saturation, as seen in Fig. 5.

In our low-temperature heat capacity data (Fig. 4), we observe no evidence of a Schottky-type anomaly. We would expect a Schottky feature to occur if the 8*a* site were split into multiple sites, each displaced slightly and symmetrically from the $(\frac{1}{8}, \frac{1}{8}, \frac{1}{8})$ and equivalent positions. Such multiple sites would be energetically equivalent, or nearly so, causing tunnel splitting of the ground and possibly even excited vibrational states. Evidence for splitting has been detected in $Eu_8Ga_{16}Ge_{30}$ from nuclear density maps derived from neutron diffraction data,[17] and splitting has been predicted in $Sr_8Ga_{16}Ge_{30}$ by means of first-principles calculations.[27] Based on the heat capacity data in Fig. 4, though, we conclude that the 8*a* site in $VAl_{10.1}$ is either not split, or that any splitting results in a very small tunneling gap, less than 10 μeV. This implies that the effective potential is a single well, the minimum of which is broad and flat. Hence, the low-frequency modes of the 8*a* atoms are indeed best described as "rattling."

To our knowledge, the strong downward concavity of $\langle u^2\rangle_{\rm iso}$ that we observe in $VAl_{10.1}$ has not been seen for rattling atoms in other materials. In our search of the literature, we found $\langle u^2\rangle_{\rm iso}$ versus T data (measured via neutron diffraction) for the La and Tl rattling atoms in the filled skutterudites $La_{0.75}Fe_3CoSb_{12}$ and $Tl_{0.22}CoSb_{12}$,[13,14] for the K rattling atom in the β-pyrochlore oxide KOs_2O_6,[25] for the Eu, Sr, and Ba

rattling atoms in the clathrates $X_8Ga_{16}Ge_{30}$ (X = Eu, Sr, Ba), $Ba_8Ga_{16}Si_{30}$, and $Sr_8Zn_8Ge_{38}$,[17,64] and for the Na rattling atom in the clathrate $Na_{24}Si_{136}$.[65] For all of these materials, with the exception of $Eu_8Ga_{16}Ge_{30}$, $\langle u^2\rangle_{\rm iso}$ increases approximately *linearly* with temperature in the range $30 < T < 300$ K. This is demonstrated in Fig. 7(a), where we reproduce literature data for $Sr_8Ga_{16}Ge_{30}$,[64] KOs_2O_6,[25] and $Eu_8Ga_{16}Ge_{30}$.[17] Only the clathrate $Eu_8Ga_{16}Ge_{30}$ is different in that $\langle u^2\rangle_{\rm iso}$ seems nearly temperature independent above 40 K. Interestingly, for both $Eu_8Ga_{16}Ge_{30}$ and $Sr_8Ga_{16}Ge_{30}$, $\langle u^2\rangle_{\rm iso}$ appears to *increase* as the temperature is decreased below ~30 K.

Ostensibly, the linear T dependence of $\langle u^2\rangle_{\rm iso}$ implies that the rattling is harmonic. This is why these data are usually interpreted in terms of a harmonic Einstein model. Other measurements for the same and similar materials, however, show direct evidence for anharmonicity of the rattling. Here, we cite four examples: (1) Nuclear density maps of the Eu site in $Eu_8Ga_{16}Ge_{30}$ show evidence for fourfold splitting, at least for temperatures near 40 K.[17] (2) Thermodynamic measurements for $Sr_8Ga_{16}Ge_{30}$, $Ba_8Ga_{16}Si_{30}$, and $Sr_8Zn_8Ge_{38}$ show that the mode-averaged Grüneisen parameter Γ increases with decreasing temperature, with values reaching $\Gamma \sim 10$ at 25 K.[64] (3) Neutron scattering experiments done on the β-pyrochlore oxides AOs_2O_6 (A = K, Rb, Cs) (Ref. 66) show that for all three compounds, the inelastic peak associated with the alkali-metal rattling ion shifts monotonically to lower frequencies as the temperature is decreased. (4) NMR measurements done on KOs_2O_6 show an unusual temperature dependence of the K-site nuclear relaxation that has been explained in terms of a highly anharmonic, low-frequency phonon.[62,67]

The data shown in Fig. 7(a) (and other data not shown here), together with the above-mentioned evidence of anharmonicity, suggests that the rattling can be anharmonic, yet the corresponding $\langle u^2\rangle_{\rm iso}$ can have a quasilinear temperature dependence that might easily be misinterpreted as harmonic. In what follows, we show that this can indeed occur for a local anharmonic vibration that is characterized by a double-well potential. For at least the Eu-filled clathrate $Eu_8Ga_{16}Ge_{30}$, there are data suggesting that a multiple-well model is a more appropriate description than a single well. Specifically, the nuclear density map for the rattling Eu atom, as determined from single-crystal neutron diffraction, shows a fourfold splitting of the Eu nucleus at 40 K.[17] Also, for $Sr_8Ga_{16}Ge_{30}$, density functional theory (DFT) calculations suggest that the Sr atom rattles in a multiple-well potential.[27]

We model the rattling modes as a particle in a one-dimensional double-well potential $V(u) = -\frac{1}{2}\alpha m\omega_4^2 u^2 + \frac{1}{4}(m^2\omega_4^3/\hbar)u^4$, where α is a positive constant and ω_4 is the characteristic frequency of the quartic contribution. Although here we use a 2–4 potential, qualitatively similar results are obtained by choosing 2–6, 2–8, etc. potentials. By using the previously described methodology, we solve the Schrödinger equation numerically for particular values of α, $\theta_4 = \hbar\omega_4/k_B$, and m and then compute $\langle u^2\rangle_{\rm iso} = \langle u^2\rangle_0 + \sum_n p_n\langle\Psi_n|u^2|\Psi_n\rangle$. Figure 7(b) shows schematics of the interatomic potentials with the eigenenergies superimposed. The calculated values of $\langle u^2\rangle_{\rm iso}$ are relative to the $u = 0$ positions shown in Fig. 7(b). In other words, we use a single-site model. The reason is that a single-site model is normally used to deduce $\langle u^2\rangle_{\rm iso}$ values from diffraction data. As best as we can tell, this is the case for all of the data shown in Fig. 7(a).

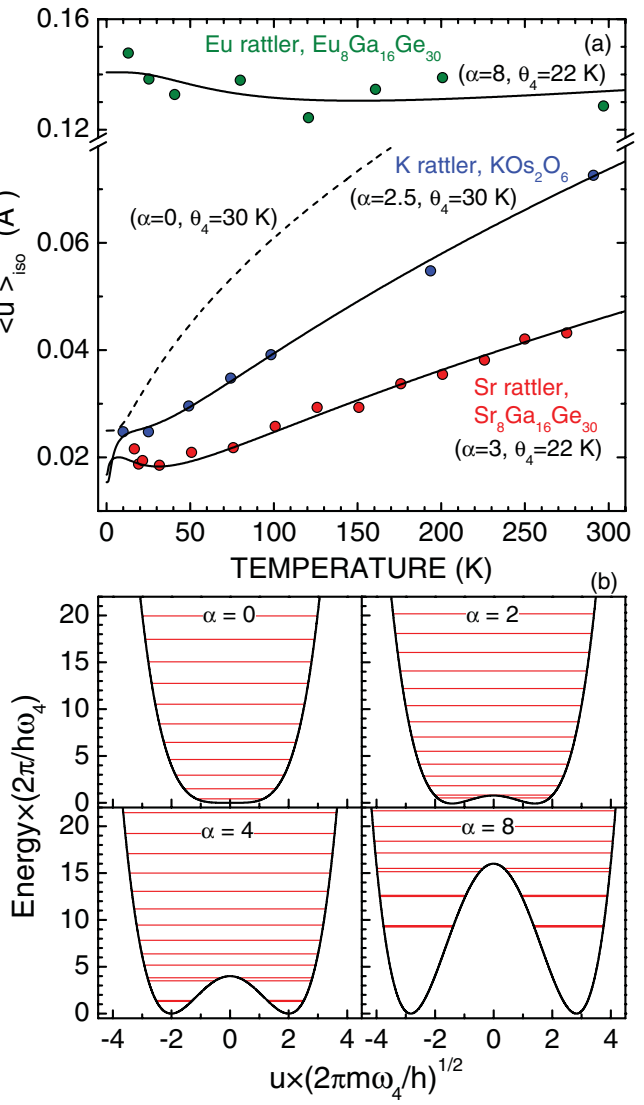

FIG. 7. (Color online) (a) Temperature dependence of $\langle u^2\rangle_{\rm iso}$ for rattling atoms in the indicated materials. Data are reproduced from Refs. 13,25,64, and 17. The curves are computed for a 2–4 double-well potential, using the mass of the specified rattler and the indicated values of α and θ_4. The $\alpha = 0$ dashed curve (calculated for a K atom) shows how the T dependence differs for purely quartic vs. double-well potentials. (b) Schematics of the interatomic potentials for the indicated values of α, plotted in terms of dimensionless energy $E/\hbar\omega_4$ and dimensionless displacement $\xi = u\sqrt{(m\omega_4/\hbar)}$. Eigenenergies are denoted by the horizontal lines. Thin lines denote a single energy level, whereas thick lines denote two levels with a small tunnel splitting.

As shown in Fig. 7(a), the simple double-well model captures qualitatively the range of temperature dependences observed in these literature data. This includes the quasilinear T dependence at high temperatures for the K pyrochlore and Sr clathrate, the temperature independence at high temperatures for the Eu clathrate, and the upturn in $\langle u^2\rangle_{\rm iso}$ at low temperatures for the Eu and Sr clathrates. In reality, of course, the potential might be considerably more complicated

than our simple model, as suggested, for example, by DFT calculations done for $Sr_8Ga_{16}Ge_{30}$.[27] Also, depending on the rattling site symmetry, the mean-square displacements may be anisotropic, meaning that the values of $\langle u^2\rangle_{\rm iso}$ shown in Fig. 7(a) are an approximation. Nonetheless, we can gain physical insight from this simple model. As the double well becomes deeper, the magnitude of $\langle u^2\rangle_{\rm iso}$ increases and its temperature dependence changes dramatically. The increase in magnitude results from the broadening of the potential well in the presence of the destabilizing quadratic term. This effect is most pronounced near the ground state due to the splitting of the equilibrium position. For the purely quartic potential, $\langle u^2\rangle_{\rm iso} \propto T^{1/2}$ in the high-temperature limit.[62] As the value of α increases and the depth of the double well grows, the high-temperature dependence changes to quasilinear (for $\alpha = 2$–3) to almost temperature independent, but with a broad and shallow minimum (for $\alpha = 6$–8).

Notice that we need two parameters to describe the double-well potentials (θ_4 and α), so the value of θ_4 can not be compared directly to characteristic temperatures deduced from experiment. To estimate an experimental characteristic temperature, we must consult with the schematics in Fig. 7(b). The ordinate of Fig. 7(b) shows the energy expressed in multiples of $\hbar\omega_4 = k_B\theta_4$. Notice in the figure that for $\alpha = 4$, the energy gap between the ground and first excited states is $k_B\theta_4 \approx 3$, whereas for $\alpha = 2$ it is $0.5k_B\theta_4$. Thus, for the Sr clathrate, which we model using $\alpha = 3$, in the limit of low temperatures we expect to measure a characteristic temperature of $\theta \approx 2\theta_4 = 44$ K. This is in good agreement with the values deduced from heat capacity ($\theta = 53$ K) (Ref. 17) and Raman spectroscopy ($\theta = 46$ K).[68]

The above analysis suggests that for at least some materials, the rattling atoms reside in strongly anharmonic multiple-well potentials. At present, we can not comment on the prevalence of multiple wells among rattling-mode materials. However, it does appear that the anharmonicity in $VAl_{10.1}$ is different than in the materials shown in Fig. 7(a). Specifically, the Al atoms seem to rattle in a boxlike (sextic) potential rather than a multiple-well potential.

In view of the anharmonicity of the 8*a* vibrations, the large values of γ^V_{RM} and γ^G_{RM} deduced from the elastic constant and Grüneisen data are not surprising. Although such large couplings are rare, they are not unprecedented. As examples, we can cite (1) the low–frequency ($\theta \approx 40$ K) resonant modes associated with the ⟨100⟩ split-dumbbell interstitial defects in neutron-irradiated Cu, which have $\gamma^G \sim 40$–100,[69] (2) tunneling states associated with impurities in alkali halide crystals, which can have γ values as large at 300,[70] and (3) the collective vibrations of stringlike arrays of atoms in metallic glasses, for which $\gamma^G \sim 50$.[59] Also, as previously mentioned, the rattling-mode clathrates $Sr_8Ga_{16}Ge_{30}$, $Ba_8Ga_{16}Si_{30}$, and $Sr_8Zn_8Ge_{38}$ all have $\Gamma \sim 10$ at 25 K,[64] which implies large values of γ^V_{RM}.

One of the most interesting and important questions toward the fundamental understanding of rattling modes is the origin of the strong coupling and anharmonicity. This has been investigated by several groups and for several different materials: Tse and co-workers[33,34] for Kr-filled clathrate hydrates, Koza *et al.*[35] for La and Ce-filled Fe_4Sb_{12} skutterudites, and Christensen *et al.*[36] for the clathrate $Ba_8Ga_{16}Ge_{30}$. The main conclusion from all of these studies was that the coupling of the guest modes to the acoustic phonons, and in fact the existence of the anharmonic potential, results from avoided crossings of the localized guest modes with the acoustic-phonon branches having the same symmetry.

The avoided crossing of the guest and acoustic branches is expected to occur inside the Brillouin zone, not at the zone center or boundary. It is therefore surprising that the rattler-phonon coupling appears so strongly in the $VAl_{10.1}$ elastic constant data, considering that the ultrasonic methods used here probe only the $k = 0$ acoustic modes. By using the rattling-mode frequency $\omega_{RM,6}$ deduced from heat capacity data, together with the values of the elastic constants, we can crudely estimate the anticrossing points in $VAl_{10.1}$. Assuming that the acoustic modes follow a linear dispersion, and that the rattling mode is dispersionless, the wave vector at the anticross point is $k_{\rm ACP} = \omega_{RM,6}/v$, where v is the sound velocity. For the anticrossing of the longitudinal acoustic (LA) modes, we estimate $k_{\rm ACP} \approx 0.04$ Å^{-1}, and for the transverse acoustic (TA) modes $k_{\rm ACP} \approx 0.07$ Å^{-1}.

For wave numbers above the anticross point $k > k_{\rm ACP}$, the TA and LA group velocities are expected to be nearly zero, in which case these phonons will be inefficient at transporting heat. Hence, one possible strategy for reducing the lattice thermal conductivity, and thus improving the figure of merit for thermoelectric applications, is to decrease $k_{\rm ACP}$ so that only a small number of acoustic-phonon states are capable of effectively transporting heat. In principle, $k_{\rm ACP}$ can be minimized by reducing the frequency of the rattling modes and/or stiffening the lattice such that the LA and TA velocities are increased.

B. Coupling of the rattling modes to the electrons

Resistivity saturation behavior similar to that seen in $VAl_{10.1}$ (Fig. 5) has also been observed in other rattling-mode materials, for example, β-pyrochlores AOs_2O_6 (A = Cs, Rb, K),[26,71–73] and the filled skutterudite $PrOs_4Sb_{12}$.[29] Mahan and Sofo[57] and Dahm and Ueda[62] have proposed that saturation-type behavior is expected for the scattering of electrons by strongly anharmonic vibrations. On the other hand, resistivity saturation is a common behavior for poor metals,[63] so that the relationship between the saturation and the rattling mode, if any, is unclear. This question could be answered most directly by somehow preparing these materials without the rattling modes. For $VAl_{10+\delta}$, however, we have so far been unable to do this.

We attempt to answer this question by examining the mean-free path of the conduction electrons l. Figure 8 shows the temperature dependence of l, as estimated from our electrical resistivity and thermal conductivity data. To calculate l, we assumed a free-electron Fermi gas, so that using the resistivity data $l = \pi^2 k_B^2/\gamma v_F e^2 \rho$, whereas using the thermal conductivity data $l = 3\kappa_e/\gamma v_F T$. Here, γ is the Sommerfeld coefficient determined from heat capacity data, κ_e is the electronic thermal conductivity, and v_F is the electron velocity at the Fermi level, which we assumed equal to that for pure Al, $v_F = 2 \times 10^6$ m/s.

As shown in Fig. 8, from our room-temperature data, we estimated $l \sim 2.5$ Å. Using the saturation resistivity of

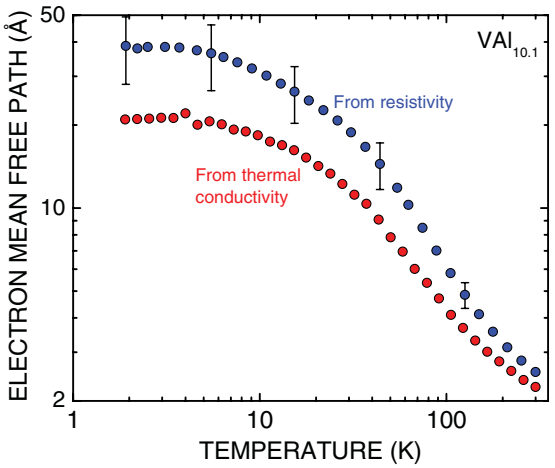

FIG. 8. (Color online) Temperature dependence of the electron mean-free path, as calculated from resistivity and thermal conductivity data. The resistivity-derived data were determined by averaging measurements on three different samples. Representative error bars are shown for several temperatures.

$\rho_{max} = 188\ \mu\Omega$ cm, the value is $l = 1.3$ Å. These values are comparable to the ∼2.7 Å average interatomic spacing in $VAl_{10.1}$, but are almost an order of magnitude smaller than the ∼16 Å spacing between the *occupied* rattling atom sites. Thus, the resistivity saturation in $VAl_{10.1}$ evidently corresponds to electron-phonon scattering by nearest-neighbor atoms, i.e., the usual Ioffe-Regel limit,[74] rather than by scattering from the rattling atoms.

For low temperatures, we estimated $l \sim 20$–40 Å. These values are small enough that extrinsic scattering from grain boundaries can be excluded. However, given the purity of our samples, we can not rule out scattering from impurities, or from crystal defects. Nonetheless, it is interesting that these values of l are comparable to the ∼16 Å distance between occupied rattling atom sites in $VAl_{10.1}$. (Note that this value may be 50% too small, given the uncertainly about the $VAl_{10+\delta}$ phase composition.) Thus, we must keep open the possibility that the 8*a* atoms, rattling anharmonically in their ground states, strongly scatter electrons and thus contribute significantly to the small mean-free path at 0 K. In this sense, the occupied rattling sites may be akin to point defects. Unlike point defects, however, the rattling atoms contribute strongly to the temperature dependence of the resistivity, especially at low temperatures. The effect is particularly evident for $T < 12$ K, where the interaction of the sextic vibration with the electrons dominates the T dependence of the resistivity, and evidently results in a $\rho(T) \propto T^3$ dependence below 6 K.

The broad, gradually sloping plateau in the thermal conductivity of $VAl_{10.1}$ (Fig. 6) is qualitatively similar to plateaus observed previously for glasses, for crystalline but disordered solids,[75] and for other rattling-mode materials such as clathrates[17,23] and filled skutterudites.[13,14] The plateau is usually interpreted as a signature of disorder, which results in scattering of the heat-carrying phonons and/or electrons. In the case of glasses and disordered crystals, the nature of the disorder seems clear, namely, the absence of long-range translational and/or orientational symmetry (the latter being particularly relevant for molecular-based materials). In the case of rattling-mode materials, the disorder is evidently not usually of the static structural type. Rather, it is dynamic disorder associated with the large-amplitude vibrations of the rattling atoms. For poorly conducting metals and/or semiconductors where heat is transported mainly by the phonons, this is normally explained in terms of resonant scattering of long-wavelength phonons by the low-energy rattling modes. The recent work by Tse *et al.*,[34] Koza *et al.*,[35] and Christensen and co-workers[36] indicates that the poor thermal conductivity is better explained in terms rattler-acoustic mode coupling due to avoided crossings.

For metallic rattling-mode metals where the thermal conductivity is mainly electronic, such as $VAl_{10.1}$ and $Na_{24}Si_{136}$,[23] the connection between the plateau and the rattling seems less clear. The reason is that the plateau temperature is above the range where the rattling mode dominates $\rho(T)$. It is also important to note that a plateau in $\kappa(T)$ will occur whenever $\rho(T)$ varies linearly with temperature. Of course, this is the usual T dependence of ρ associated with electron-harmonic phonon scattering in the high-temperature limit. Thus, it should come as no surprise that thermal conductivity plateaus are ubiquitous in metallic crystals.

Based on the available data, then, it appears that the main difference between $\kappa(T)$ for rattling-mode metals and $\kappa(T)$ for "normal" metals is the absence of a peak for the rattling materials. For normal metals, the peak occurs at temperatures below the plateau and is associated with the transition from defect-dominated electron scattering at low temperatures to phonon-dominated scattering at higher temperatures.[76] At present, we do not know why a peak is virtually absent from the known rattling-mode metals. However, one possibility is that the rattling modes are akin to a large defect concentration, which suppresses completely the $\kappa(T)$ peak.

V. SUMMARY AND CONCLUDING REMARKS

Presently, there are two main reasons for the interest in rattling modes: (1) their ability to scatter heat-carrying acoustic phonons, and hence their potential role in development of improved thermoelectric materials utilizing the "electron crystal-phonon glass" concept, and (2) their apparent ability to facilitate electron-electron and electron-phonon coupling, thereby promoting superconductivity and electron mass enhancement. Although $VAl_{10.1}$ is neither a promising thermoelectric material nor a superconductor with high T_c or heavy electrons, it is nonetheless a useful model compound to study the enhanced couplings associated with rattling modes.

Two characteristics of the rattling in $VAl_{10.1}$ seem to make it remarkable even among the growing ranks of rattling-mode materials. First, the rattling frequency of the 8*a* Al atom, $\theta_{RM,6} = 21$ K, is among the lowest of all known rattling-mode materials. This is surprising considering the light mass of the Al rattler compared to rattlers in other materials. Second, in qualitative terms, the rattling Al atom behaves like a particle in a box. This is clear from the temperature dependence of the $\langle u^2 \rangle_{iso}$ data, which is concave down to the abscissa. Quantitatively, these data can be described in terms of a dispersionless sixth-order vibration, with negligible contributions from harmonic or quartic terms. Additional

evidence for the boxlike character comes from heat capacity measurements down to 100 mK, which show no Schottky anomaly that would signify tunnel splitting of the ground vibrational state. At present, the rattling mode in $VAl_{10.1}$ is the only one we know of that seems to be associated with a broad, flat potential that allows for large *dynamic* atomic displacements even in the ground state. Potentials of this shape may be of particular interest because they have been predicted to enhance phonon-mediated electron-electron attraction and Cooper-pair formation.[38]

The large coupling of the Al rattling mode to long-wavelength acoustic phonons, as characterized by mode Grüneisen parameters $\gamma_{RM}^{G} = 24$ and $\gamma_{RM}^{V} = 54$–73, is also extraordinary. Because of the uncertainty in our sample composition, we consider these values to be lower bounds. Although the body of literature now shows ample evidence for strong anharmonicity and rattling-mode–acoustic-phonon coupling, to our knowledge this is the first time that the coupling strength has been quantified. Among all materials, only a few examples of such strong coupling are known. Based on the present data, it seems reasonable to conclude that the rattling-mode–acoustic-phonon coupling in $VAl_{10.1}$ can be explained in terms of avoided crossings of the rattler and acoustic-phonon branches.

At low temperatures, the rattling modes in $VAl_{10.1}$ couple strongly to the electrons and dominate the temperature dependence of the resistivity. For $T < 12$ K, $\rho(T)$ can be explained in terms of electron scattering from a damped sextic oscillator, where the damping is assumed to arise from the strong electron-phonon interaction. For $T < 6$ K, this coupling results in a T^3 dependence of the resistivity. At higher temperatures, the rattling modes seem to have little connection to the saturation of the electrical resistivity. Likewise, although the temperature dependence of the thermal conductivity shows a plateau that is akin to that seen for glasses, disordered crystals, and other rattling-mode materials, it does not appear to be associated with the rattling.

ACKNOWLEDGMENTS

This work was supported in part by the Department of Energy's Laboratory Directed Research and Development Program. The authors thank E. K. H. Salje for several informative discussions.

[1] D. K. Campbell, S. Flach, and Y. S. Kivshar, Phys. Today **57**(1), 43 (2004).
[2] P. H. Dederichs, C. Lehmann, and A. Scholz, Phys. Rev. Lett. **31**, 1130 (1973).
[3] P. N. Ram, Radiat. Eff. Defects Solids **118**, 1 (1991).
[4] A. J. Sievers and S. Takeno, Phys. Rev. Lett. **61**, 970 (1988).
[5] J. B. Page, Phys. Rev. B **41**, 7835 (1990).
[6] R. S. MacKay and S. Aubry, Nonlinearity **7**, 1623 (1994).
[7] D. Bonart, A. P. Mayer, and U. Schröder, Phys. Rev. Lett. **75**, 870 (1995).
[8] E. Trías, J. J. Mazo, and T. P. Orlando, Phys. Rev. Lett. **84**, 741 (2000).
[9] P. Binder, D. Abraimov, A. V. Ustinov, S. Flach, and Y. Zolotaryuk, Phys. Rev. Lett. **84**, 745 (2000).
[10] H. S. Eisenberg, Y. Silberberg, R. Morandotti, A. R. Boyd, and J. S. Aitchison, Phys. Rev. Lett. **81**, 3383 (1998).
[11] M. Sato, B. E. Hubbard, and A. J. Sievers, Rev. Mod. Phys. **78**, 137 (2006).
[12] M. E. Manley, M. Yethiraj, H. Sinn, H. M. Volz, A. Alatas, J. C. Lashley, W. L. Hults, G. H. Lander, and J. L. Smith, Phys. Rev. Lett. **96**, 125501 (2006).
[13] B. C. Sales, D. Mandrus, B. C. Chakoumakos, V. Keppens, and J. R. Thompson, Phys. Rev. B **56**, 15081 (1997).
[14] B. C. Sales, B. C. Chakoumakos, and D. Mandrus, Phys. Rev. B **61**, 2475 (2000).
[15] T. Goto, Y. Nemoto, T. Yamaguchi, T. Yanagisawa, T. Ueno, T. Watanabe, N. Takeda, O. Suzuki, H. Kitazawa, H. Sugawara, and H. Sato, Phys. B (Amsterdam) **383**, 115 (2006).
[16] Y. Nakai, K. Ishida, H. Sugawara, D. Kikuchi, and H. Sato, Phys. Rev. B **77**, 041101 (2008).
[17] B. C. Sales, B. C. Chakoumakos, R. Jin, J. R. Thompson, and D. Mandrus, Phys. Rev. B **63**, 245113 (2001).
[18] I. Zerec, V. Keppens, M. A. McGuire, D. Mandrus, B. C. Sales, and P. Thalmeier, Phys. Rev. Lett. **92**, 185502 (2004).
[19] T. Goto, Y. Nemoto, T. Yamaguchi, M. Akatsu, T. Yanagisawa, O. Suzuki, and H. Kitazawa, Phys. Rev. B **70**, 184126 (2004).
[20] T. Watanabe, T. Yamaguchi, Y. Nemoto, T. Goto, N. Takeda, O. Suzuki, and H. Kitazawa, J. Magn. Magn. Mater. **310**, 280 (2007).
[21] S. Paschen, V. H. Tran, M. Baenitz, W. Carrillo-Cabrera, Y. Grin, and F. Steglich, Phys. Rev. B **65**, 134435 (2002).
[22] M. Schmidt, P. G. Radaelli, M. J. Gutmann, S. J. L. Billinge, N. Hur, and S. W. Cheong, J. Phys.: Condens. Matter **16**, 7287 (2004).
[23] M. Beekman, W. Schnelle, H. Borrmann, M. Baitinger, Y. Grin, and G. S. Nolas, Phys. Rev. Lett. **104**, 018301 (2010).
[24] Z. Hiroi, S. Yonezawa, T. Muramatsu, J. I. Yamaura, and Y. Muraoka, J. Phys. Soc. Jpn. **74**, 1255 (2005).
[25] J. I. Yamaura, S. Yonezawa, Y. Muraoka, and Z. Hiroi, J. Solid State Chem. **179**, 336 (2006).
[26] Y. Nagao, J. I. Yamaura, H. Ogusu, Y. Okamoto, and Z. Hiroi, J. Phys. Soc. Jpn. **78**, 064702 (2009).
[27] G. K. H. Madsen and G. Santi, Phys. Rev. B **72**, 220301 (2005).
[28] F. M. Grosche, H. Q. Yuan, W. Carrillo-Cabrera, S. Paschen, C. Langhammer, F. Kromer, G. Sparn, M. Baenitz, Y. Grin, and F. Steglich, Phys. Rev. Lett. **87**, 247003 (2001).
[29] E. D. Bauer, N. A. Frederick, P.-C. Ho, V. S. Zapf, and M. B. Maple, Phys. Rev. B **65**, 100506 (2002).
[30] M. Brühwiler, S. M. Kazakov, J. Karpinski, and B. Batlogg, Phys. Rev. B **73**, 094518 (2006).
[31] Z. Hiroi, S. Yonezawa, Y. Nagao, and J. Yamaura, Phys. Rev. B **76**, 014523 (2007).
[32] S. Sanada, Y. Aoki, H. Aoki, A. Tsuchiya, D. Kikuchi, H. Sugawara, and H. Sato, J. Phys. Soc. Jpn. **74**, 246 (2005).
[33] J. S. Tse, V. P. Shpakov, V. V. Murashov, and V. R. Belosludov, J. Chem. Phys. **107**, 9271 (1997).

[34]J. S. Tse, D. D. Klug, J. Y. Zhao, W. Sturhahn, E. E. Alp, J. Baumert, C. Gutt, M. R. Johnson, and W. Press, Nat. Mater. **4**, 917 (2005).
[35]M. M. Koza, M. R. Johnson, R. Viennois, H. Mutka, L. Girard, and D. Ravot, Nat. Mater. **7**, 805 (2008).
[36]M. Christensen, A. B. Abrahamsen, N. B. Christensen, F. Juranyi, N. H. Andersen, K. Lefmann, J. Andreasson, C. R. H. Bahl, and B. B. Iversen, Nat. Mater. **7**, 811 (2008).
[37]J. Kuneš and W. E. Pickett, Phys. Rev. B **74**, 094302 (2006).
[38]T. Hotta, J. Phys. Soc. Jpn. **77**, 103711 (2008).
[39]A. D. Caplin, G. Grüner, and J. B. Dunlop, Phys. Rev. Lett. **30**, 1138 (1973).
[40]J. R. Cooper, Phys. Rev. B **9**, 2778 (1974).
[41]A. D. Caplin and L. K. Nicholson, J. Phys. F: Met. Phys. **8**, 51 (1978).
[42]G. J. Legg and P. C. Lanchester, J. Phys. F: Met. Phys. **8**, 2125 (1978).
[43]T. Claeson and J. Ivarsson, Commun. Phys. **2**, 53 (1977).
[44]A. E. Ray and J. F. Smith, Acta Crystallogr. **10**, 604 (1957).
[45]P. J. Brown, Acta Crystallogr. **10**, 133 (1957).
[46]Y. Verbovytsky, K. Latka, and K. Tomala, J. Alloys Compd. **442**, 334 (2007).
[47]J. Chi, Y. Li, W. Gou, V. Goruganti, K. Rathnayaka, and J. H. R. Jr., Phys. B (Amsterdam) **403**, 1426 (2008).
[48]A. C. Larson and R. B. Von Dreele, Los Alamos National Laboratory Report No. LAUR 86-748, 2004 (unpublished).
[49]B. H. Toby, J. Appl. Crystallogr. **34**, 210 (2001).
[50]G. M. Schmiedeshoff, A. W. Lounsbury, D. J. Luna, S. J. Tracy, S. J. Schramm, S. W. Tozer, V. F. Correa, S. T. Hannahs, T. P. Murphy, E. C. Palm, A. H. Lacerda, S. L. Bud'ko, P. C. Canfield, J. L. Smith, J. L. Lashley, and J. C. Cooley, Rev. Sci. Instrum. **77**, 123907 (2006).
[51]A. Migliori, J. L. Sarrao, W. M. Visscher, T. M. Bell, M. Lei, Z. Fisk, and R. G. Leisure, Phys. B (Amsterdam) **183**, 1 (1993).
[52]R. G. Leisure and F. A. Willis, J. Phys.: Condens. Matter **9**, 6001 (1997).
[53]D. J. Safarik, A. Llobet, and J. Lashley (unpublished).
[54]A. Lawson, J. Goldstone, B. Cort, R. Sheldon, and E. Foltyn, J. Alloys Compd. **213-214**, 426 (1994).
[55]B. T. M. Willis and A. W. Pryor, *Thermal Vibrations in Crystallography* (Cambridge University Press, Cambridge, UK, 1975).
[56]J. G. Dash, D. P. Johnson, and W. M. Visscher, Phys. Rev. **168**, 1087 (1968).
[57]G. D. Mahan and J. O. Sofo, Phys. Rev. B **47**, 8050 (1993).
[58]B. Mühlschlegel, Z. Phys. **155**, 313 (1959).
[59]D. J. Safarik and R. B. Schwarz, Phys. Rev. B **80**, 094109 (2009).
[60]D. C. Wallace, *Thermodynamics of Crystals* (Dover, New York, 1972).
[61]D. C. Wallace, Phys. Rev. **162**, 776 (1967).
[62]T. Dahm and K. Ueda, Phys. Rev. Lett. **99**, 187003 (2007).
[63]H. Wiesmann, M. Gurvitch, H. Lutz, A. Ghosh, B. Schwarz, M. Strongin, P. B. Allen, and J. W. Halley, Phys. Rev. Lett. **38**, 782 (1977).
[64]L. Qiu, I. P. Swainson, G. S. Nolas, and M. A. White, Phys. Rev. B **70**, 035208 (2004).
[65]M. Beekman, R. P. Hermann, A. Möchel, F. Juranyi, and G. S. Nolas, J. Phys.: Condens. Matter **22**, 355401 (2010).
[66]H. Mutka, M. M. Koza, M. R. Johnson, Z. Hiroi, J.-I. Yamaura, and Y. Nagao, Phys. Rev. B **78**, 104307 (2008).
[67]M. Yoshida, K. Arai, R. Kaido, M. Takigawa, S. Yonezawa, Y. Muraoka, and Z. Hiroi, Phys. Rev. Lett. **98**, 197002 (2007).
[68]G. S. Nolas and C. A. Kendziora, Phys. Rev. B **62**, 7157 (2000).
[69]J. Holder, A. V. Granato, and L. E. Rehn, Phys. Rev. B **10**, 363 (1974).
[70]*Thermal Expansion-1971 Proceedings of the 1971 Thermal Expansion Symposium*, edited by M. G. Graham and H. E. Hagy (American Institute of Physics, New York, 1972).
[71]Z. Hiroi, S. Yonezawa, J.-I. Yamaura, T. Muramatsu, and Y. Muraoka, J. Phys. Soc. Jpn. **74**, 1682 (2005).
[72]S. Yonezawa, Y. Muraoka, Y. Matsushita, and Z. Hiroi, J. Phys. Soc. Jpn. **73**, 819 (2004).
[73]S. Yonezawa, Y. Muraoka, and Z. Hiroi, J. Phys. Soc. Jpn. **73**, 1655 (2004).
[74]M. Gurvitch, Phys. Rev. B **24**, 7404 (1981).
[75]R. O. Pohl, X. Liu, and R. S. Crandall, Curr. Opin. Solid State Mater. Sci. **4**, 281 (1999).
[76]R. Berman, *Thermal Conduction in Solids* (Oxford University Press, New York, 1976).